JCI insight

Modulation of the effects of Class-Ib antiarrhythmics on cardiac NaV1.5-encoded channels by accessory NaVβ subunits

Wandi Zhu, … , Jeanne M. Nerbonne, Jonathan R. Silva

JCI Insight. 2021. https://doi.org/10.1172/jci.insight.143092.

Research In-Press Preview Cardiology Therapeutics

Graphical abstract

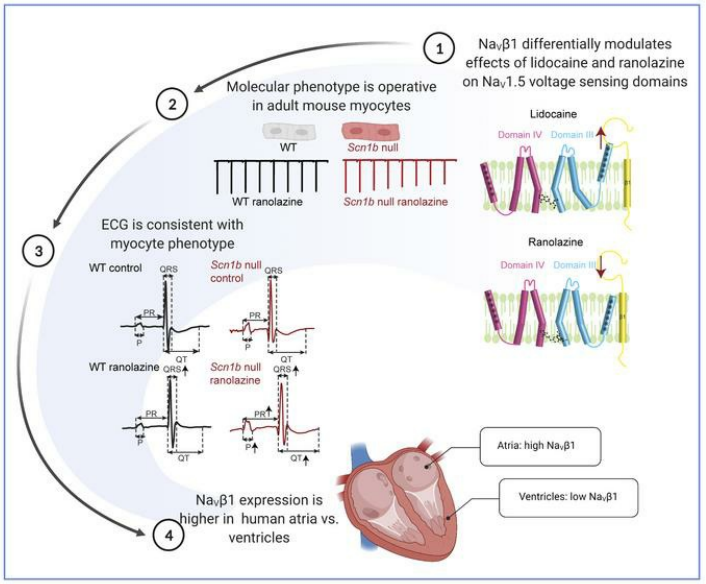

Find the latest version:

https://jci.me/143092/pdf

Title: Modulation of the effects of Class-Ib antiarrhythmics on cardiac Nav1.5-encoded channels by accessory Navβ subunits

Authors: Wandi Zhu, PhD[1, 2], Wei Wang, PhD[3], Paweorn Angsutararux[1], Rebecca L. Mellor[3], Lori L. Isom, PhD[5], Jeanne M. Nerbonne, PhD[3, 4], Jonathan R. Silva, PhD[1]

1. Department of Biomedical Engineering, Washington University in St. Louis, Missouri, 63130, United States
2. Department of Medicine, Brigham and Women's Hospital, Boston, Massachusetts, 02115, United States
3. Department of Internal Medicine, Washington University in St. Louis, St. Louis, Missouri, 63130, United States
4. Department of Developmental Biology, Washington University in St. Louis, St. Louis, Missouri, 63130, United States
5. Department of Pharmacology, University of Michigan, Ann Arbor, Michigan, 48109, United States

Corresponding authors:

Jonathan Silva, PhD, Associate Professor of Biomedical Engineering, Washington University in St. Louis, St. Louis, Missouri, 63130; email: jonsilva@wustl.edu, phone: 314-935-8837

Jeanne Nerbonne, PhD, Professor of Medicine and Developmental Biology, Washington University in St. Louis, St. Louis, Missouri, 63110; email: jnerbonne@wustl.edu, phone: 314-362-2564

Abstract:

Native myocardial voltage-gated sodium (Na_V) channels function in macromolecular complexes comprising a pore-forming (α) subunit and multiple accessory proteins. Here, we investigated the impact of accessory Na_Vβ1 and Na_Vβ3 subunits on the functional effects of two well-known Class-Ib antiarrhythmics, lidocaine and ranolazine, on the predominant Na_V channel α subunit, Nav1.5, expressed in mammalian heart. We show that both drugs stabilize the activated conformation of the voltage-sensor of in Domain-III (DIII-VSD) in Na_V1.5. In the presence of Na_Vβ1, the effect of lidocaine on the DIII-VSD was enhanced, whereas the effect of ranolazine was abolished. Mutating the main Class-Ib drug binding site, F1760, affected but did not abolish, the modulation of drug block by Navβ1/β3. Recordings from adult mouse ventricular myocytes demonstrated that *Scn1b* (Navβ1) loss of differentially affected the potencies of lidocaine and ranolazine. *In vivo* experiments revealed distinct ECG responses to intraperitoneal injection of ranolazine or lidocaine in WT and *Scn1b* null animals, suggesting that Na_Vβ1 modulates drug responses at the whole heart level. In human heart, we found that *SCN1B* transcript expression is three times higher in atria than ventricles, differences that could, in combination with inherited or acquired cardiovascular disease, dramatically impact patient response to Class-Ib antiarrhythmic therapies.

Introduction:

Inward Na^+ currents (I_{Na}) carried by voltage-gated (Na_V) channels underlie the initiation and propagation of action potentials in atria and ventricles(1). Functional Na_V channels reflect the assembly of the four homologous domains (DI-DIV) in the pore-forming (α) subunit that are connected by intracellular linkers. Each domain contains six transmembrane segments (S1-S6). S1-S4 form the voltage-sensing domains (VSDs). The VSDs undergo conformational changes upon membrane depolarization, which open the pore (S5-S6), enabling inward Na^+ flux(2). Native myocardial Na_V channels function in macromolecular protein complexes, containing many regulatory and anchoring proteins that differentially affect channel function and localization based on the cell type(3). $Na_V\beta$ subunits are essential components of these macromolecular complexes. There are five different types of $Na_V\beta$ subunits, $Na_V\beta1$, $Na_V\beta1B$, $Na_V\beta2$, $Na_V\beta3$, and $Na_V\beta4$. $Na_V\beta1$, $Na_V\beta1B$, and $Na_V\beta3$ interact with the Na_V α subunits non-covalently, while $Na_V\beta2$ and $Na_V\beta4$ are linked covalently through the formation of disulfide bonds(4). While Navβ1, Navβ2, $Na_V\beta3$, and $Na_V\beta4$ are transmembrane proteins, $Na_V\beta1B$ is secreted(5). Consistent with a crucial role for Navβ subunits in maintaining normal heart function, variants in the genes encoding $Na_V\beta$ subunits have been linked to cardiac rhythm disorders, including Brugada syndrome, long QT syndrome, and sick sinus syndrome(4). However, recent evidence suggests that SCN1B may not be a monogenic cause of Brugada or Sudden Arrhythmic Death Syndrome(6, 7). $Na_V\beta1$ and $Na_V\beta1B$, splice variants of *SCN1B*, are the dominant $Na_V\beta$ subunits in the mammalian heart(8).

Although $Na_V\beta$ subunits were first cloned from rat brain in the 1990's (9), the molecular interactions between $Na_V\alpha$-$Na_V\beta$ subunits have remained elusive until recently. The cryo-EM structures of the $Na_V1.4$-$Na_V\beta1$ and the $Na_V1.7$-$Na_V\beta1$-$Na_V\beta2$ complexes suggest that Navβ1 co-

assembles with Na_V α subunits near the DIII-VSD(10–12). However, the recent structure of $Na_V1.5$ revealed that Navβ1 interacts with the predominant cardiac Na_V α subunit at a distinct site or sites that are characterized by weaker binding and an unresolvable $Na_V1.5$-$Na_V\beta1$ complex(13). This difference in comparison to channels encoded by other Nav α subunits is partially due to the unique N-linked glycosylation of $Na_V1.5$ that hinders its interaction with the immunoglobulin (Ig) domain of $Na_V\beta1$(13). Intriguingly, $Na_V\beta1$ and $Na_V\beta3$ are highly homologous except in the Ig domains. Previously, optical tracking of the $Na_V1.5$ VSDs using voltage-clamp fluorometry (VCF) revealed that the Navβ3 subunit modulates both the DIII and the DIV-VSDs, while Navβ1 only modulates the DIV-VSD conformational dynamics(14, 15). Fluorescence quenching experiments showed that the DIII-VSD is in close proximity to Navβ3, but not Navβ1(14). These results suggest that $Na_V\beta1$ and $Na_V\beta3$ regulate the $Na_V1.5$ DIII-VSD differently.

The conformational changes in the VSDs are not only important for regulating channel gating; they are also essential for modulating channel interactions with drugs, including those that bind to the pore domain, such as local anesthetics(16). Previously, VCF and gating current recordings showed that, when lidocaine blocks $Na_V1.4$ channels, it stabilizes the DIII-VSD in its activated conformation(17). Moreover, we recently demonstrated that alteration of DIII-VSD conformational changes evident with long QT syndrome 3 variants, leads to channels with different mexiletine sensitivities(18, 19).

Class I antiarrhythmics modulate cardiomyocyte excitability via Na_V channel targeting. Class Ib molecules, such as lidocaine, ranolazine, and mexiletine, specifically modulate the late component of I_{Na}, resulting in shortening of the action potential duration in ventricular cardiomyocytes(20). Lidocaine has long been used to manage ventricular arrhythmias in hospital

settings(21). Ranolazine has been shown to be effective in controlling various cases of atrial fibrillation (AF)(22–24), particularly paroxysmal AF(25, 26). Recently, the RAID Trial demonstrated that ranolazine also marginally lowered the risk of recurrent ventricular tachycardia and ventricular fibrillation in high risk patients with implanted cardioverter-defibrillators(27). Although both drugs are commonly prescribed for several arrhythmias, their efficacies are highly variable. Thus, it remains an important task to understand the determinants of channel-drug interactions that contribute to this variability.

In the experiments presented here, we aimed to understand the molecular mechanisms whereby non-covalently bound Navβ subunits modulate the interaction of Class-Ib antiarrhythmics with myocardial $Na_V1.5$ channels. We further investigated the physiological significance of this modulation by assessing ranolazine and lidocaine drug blockade of native Na_V currents in mouse ventricular myocytes, probing the mRNA expression levels of Navβ subunits in human hearts and detailing the i*n vivo* electrophysiological phenotypes evident in the cardiac-specific *Scn1b* null mouse(28). Our results show a critical role for β subunits in differentially modulating the efficacy of lidocaine and ranolazine, implying that patient-to-patient differences in β-subunit expression are likely to have a significant impact on therapeutic outcomes.

Results:

Both lidocaine and ranolazine alter Na$_V$1.5 DIII-VSD dynamics

Previous studies demonstrated that lidocaine shifts the activation of the DIII-VSD in rat Na$_V$1.4 channels encoded by *Scn4a* and prominent in skeletal muscle, in the hyperpolarizing direction (16, 29, 30). Recent findings showed that a Class-Ib antiarrhythmic, mexiletine, which is similar in structure to lidocaine, also affects the DIII-VSD conformation in Na$_V$1.5 channels(18, 19). The DIII-VSD effect also determines the tonic and use-dependent properties of Class-Ib drugs(18, 19). Taken together, these observations suggest that factors that alter drug effects on the DIII-VSD would be expected to have an impact on therapeutic efficacy.

To explore this hypothesis, we first used voltage-clamp fluorometry (VCF) to assess the effects of two Class Ib antiarrhythmics, lidocaine and ranolazine (**Figure 1A**), on the DIII-VSD in heterologously expressed human Na$_V$1.5 channels, which are encoded by *SCN5A*, the predominant Na$_V$ α subunit expressed in the mammalian heart (**Figure 1B-C**). When we expressed the Nav1.5 α subunit alone in *Xenopus* oocytes, we observed a hyperpolarizing shift ($\Delta V_{1/2}$ = -24.8 ± 9.4 mV, p = 0.03) in the DIII fluorescence-voltage (F-V) curve on exposure to 10 mM lidocaine, and a similar shift ($\Delta V_{1/2}$ = -30.7 ± 7.5 mV, p = 0.05) on application of 4 mM ranolazine, suggesting that both lidocaine and ranolazine stabilize the DIII-VSD in its activated conformation (**Figure 1B-D)**. The observation of similar effects on the DIII-VSD caused by both drugs is not surprising as they share similar molecular structures (**Figure 1A**), shown previously to interact with residue F1760 in DIV-S6 (20, 31). In addition, however, the effects of lidocaine and ranolazine are not identical. Lidocaine, for example, induced a hyperpolarizing shift in the DIV F-V curve, an effect not observed with ranolazine (**Figure 1B-D**), suggesting that, despite

sharing common binding motifs on the $Na_V1.5$ α subunit, the distinct chemical structures of lidocaine and ranolazine (**Figure 1A**) uniquely regulate DIV-VSD dynamics.

$Na_V\beta1$ and $Na_V\beta3$ differentially modulate lidocaine/ranolazine effects on the DIII-VSD

We have previously shown that both $Na_V\beta1$ and $Na_V\beta3$ alter DIII-VSD dynamics during $Na_V1.5$ channel gating(14). Thus, we hypothesized that these $Na_V\beta$ subunits will also alter the effects of Class Ib antiarrhythmics on the DIII-VSD. To test this hypothesis, we co-expressed $Na_V1.5$ with the $Na_V\beta1$ or $Na_V\beta3$ subunit and measured DIII-VSD and DIV-VSD conformational changes before and after lidocaine or ranolazine application.

When we co-expressed $Na_V1.5$ with $Na_V\beta1$, we observed distinct DIII-VSD responses to lidocaine and ranolazine, respectively. Lidocaine induced a greater hyperpolarizing shift ($\Delta V_{1/2}$ = -57.6 ± 10.2 mV, p = 0.01) in DIII-FV (**Figure 2A**) when $Na_V\beta1$ was present, compared to the $Na_V1.5$ α subunit expressed alone. Exposure to ranolazine, in marked contrast, did not result in a significant DIII-FV shift ($\Delta V_{1/2}$ = -12.8 ± 16.8 mV, p = 0.53) (**Figure 2C**), suggesting that the DIII-VSD is free to move in $Na_V1.5$ channels in the presence of $Na_V\beta1$, to recover to the resting state. Although the presence of $Na_V\beta1$ increased the lidocaine effect on the DIII-VSD, $Na_V\beta1$ co-expression eliminated the ranolazine effect.

Strikingly, co-expression with the $Na_V\beta3$ subunit resulted in opposite effects on lidocaine and ranolazine interaction with the DIII-VSD. Upon lidocaine block, the DIII F-V curve was minimally shifted to more hyperpolarized potentials ($\Delta V_{1/2}$ = -25.3 ± 10.9 mV, p = 0.13) (**Figure 2B**), while the ranolazine effect on the DIII-VSD was potentiated, resulting a larger hyperpolarizing shift in the DIII F-V ($\Delta V_{1/2}$ = 58.0 ± 4.7 mV, p<0.001) (**Figure 2D**).

Additionally, the co-expression of $Na_V\beta1$ or $Na_V\beta3$ both eliminated the hyperpolarizing shift in the DIV F-V curve that was observed with the Nav1.5 α subunit expressed alone (**Figure 2A-B**), suggesting that the $Na_V\beta1$ and $Na_V\beta3$ subunits similarly alter lidocaine's effect on the DIV-VSD.

These results demonstrate that $Na_V\beta$ subunits differentially regulate lidocaine and ranolazine interactions with the DIII-VSD in heterologously expressed $Na_V1.5$ channels. Specifically, $Na_V\beta1$ enhances the effect of lidocaine but decreases the effect of ranolazine on the DIII-VSD activation, while $Na_V\beta3$ co-expression has the opposite effects on both drugs. The altered drug interactions with the DIII-VSD resulted in an enhanced block by lidocaine and reduced block by ranolazine when Nav1.5 α subunit is co-expressed with $Na_V\beta1$, compared to $Na_V\beta3$ (**Figure 3C**).

To determine whether the differential modulation of lidocaine and ranolazine block by $Na_V\beta1$ and $Na_V\beta3$ is dependent on the main local anesthetic binding site F1760(20, 31) (**Figure 3A**), we assessed drug blockade of the F1760A-mutant Nav1.5 channel in the presence of $Na_V\beta1$ or $Na_V\beta3$. As expected, the F1760A mutant channels exhibit much reduced block by lidocaine and ranolazine, compared to the WT channels (**Figure 3C, D**). However, application of 10 mM lidocaine or 4 mM ranolazine still caused significant tonic (TB) and use-dependent block (UDB) of the F1760A channels (**Figure 3D, E**). TB reflects resting-state drug block, while UDB requires prior channel opening(32). In contrast to the WT channels, the hyperpolarizing shift in the DIII F-V upon lidocaine or ranolazine block is not observed with the F1760A mutant channels (**Figure 3B**). The F1760A mutation also eliminated $Na_V\beta1$ and $Na_V\beta3$ modulation of TB by lidocaine and ranolazine, as well as UDB by lidocaine (**Figure 3D, E**). However, despite of the absence of major drug binding site, co-expression of $Na_V\beta3$ still caused stronger UDB by ranolazine, compared to $Na_V\beta1$ (**Figure 3E**). These results suggest that the effects of $Na_V\beta1/\beta3$

on lidocaine and ranolazine block are affected by the F1760 anesthetic binding site but are not completely dependent on it.

Loss of *Scn1b* expression in mouse cardiomyocytes does not affect Na_V channel gating

To further investigate how non-covalent $Na_V\beta1/\beta1B$ subunits affect the cardiomyocyte response to Class Ib antiarrhythmics, we utilized the cardiac-specific *Scn1b* null mouse model (*Scn1b*$^{flox/flox}$*/Myh6-cre*) described previously(28). First, we compared I_{Na} in left ventricular (LV) myocytes acutely dissociated from adult *Scn1b* cardiac-specific null and wild type (WT) mice. Peak I_{Na} density is increased by 28% in *Scn1b* null, compared to WT LV myocytes (*Scn1b* null: 81.3±3.6pA/pF, WT: 63.9±5.2pA/pF, p=0.017). An increase in I_{Na} density in cardiac-specific *Scn1b* null isolated from juvenile mice was previously reported(28). Consistent with the increase in current density, we also observed increased *Scn5a* transcript expression in ventricles (and atria) of the *Scn1b* null, compared to the WT, mice (**Supplement Figure 1**). Other than increasing peak current density, *Scn1b* deletion did not measurably alter other Nav channel gating properties in ventricular cardiomyocytes (**Figure 4A**), including the voltage dependences of channel activation (**Figure 4B**), steady-state inactivation (**Figure 4B**), and/or the kinetics of channel recovery from inactivation (**Figure 4C**). Notably, deleting *Scn1b* did not measurably alter the expression of other $Na_V\beta$ subunits (**Supplement Figure 1**). These results, although contrary to previously reported effects of $Na_V\beta1$on I_{Na} in heterologous expression systems, are consistent with results obtained in studies on global and cardiac-specific *Scn1b* null mice(28, 33).

Increased block of I_{Na} by ranolazine, but reduced block by lidocaine, in adult *Scn1b* null mouse ventricular myocytes

Even though Na_V channel gating was not measurably affected in cardiac-specific *Scn1b* null myocytes, we went on to determine whether the loss of *Scn1b* affects the responses of native Na_V channels to Class Ib antiarrhythmics. We examined the effects of lidocaine and ranolazine on TB and UDB of I_{Na} in LV myocytes isolated from WT and cardiac-specific *Scn1b* null mice.

The TB produced by 100 μM lidocaine was similar in WT and *Scn1b* null LV myocytes (**Figure 5A**). In marked contrast, the block of late I_{Na} by lidocaine is significantly reduced in *Scn1b* null LV myocytes (**Figure 5B**). There is also a ~3-fold reduction in lidocaine UDB in *Scn1b* null, compared with WT LV myocytes (WT: EC_{50UDB} = 9.3 μM, *Scn1b* null EC_{50UDB} = 24.8 μM) (**Figure 5E**). Conversely, ranolazine increased TB, late I_{Na} block, and UDB in *Scn1b* null, compared to WT, adult mouse LV myocytes (**Figure 5C, D, F**) (WT: EC_{50UDB} = 53.3μM, *Scn1b* null EC_{50UDB} = 36.0 μM). The differences in UDB by lidocaine between WT and *Scn1b* null myocytes depend on the frequency and duration of the depolarizing pulses (**Figure 5G**). In response to 10 μM lidocaine, I_{Na} from *Scn1b* null showed decreased UDB compared to WT myocytes at 10 Hz (25 ms duration) and 2 Hz (400 ms duration), but not 5 Hz (25 ms duration) (**Figure 5G**). In contrast, in response to 10 μM ranolazine, I_{Na} in WT myocytes showed increased UDB compared to Scn1b null myocytes at all three frequencies (**Figure 5H**). Both lidocaine and ranolazine are known to cause a hyperpolarizing shift in the voltage-dependence of steady state inactivation of cardiac I_{Na}(24, 34), indicating that drug binding promotes channel inactivation at more hyperpolarized membrane potentials. Therefore, we also compared the voltage dependence of I_{Na} inactivation in WT and *Scn1b* null LV myocytes before and after lidocaine or ranolazine application. These experiments revealed 100 μM lidocaine induced a hyperpolarizing shift in I_{Na} inactivation in WT LV myocytes and a smaller shift in *Scn1b* null LV myocytes (**Supplement Figure 2A**). Conversely, 100 μM ranolazine induced a comparable

leftward shift in the voltage dependence of inactivation of I_{Na} in WT and *Scn1b* null LV myocytes (**Supplement Figure 2B**).

Overall, these cellular studies reveal that, in adult mouse LV myocytes, the cardiac deletion of *Scn1b* results in reduced lidocaine UDB, but increased ranolazine UDB. These results are consistent with our VCF data (**Figures 1 and 2**), suggesting that the presence of $Na_V\beta1$ subunits enhances lidocaine, but reduces ranolazine, effects on the $Na_V1.5$ DIII-VSD. The reduced effects on the DIII-VSD are also consistent with the decreased UDB of I_{Na} observed in LV myocytes (**Figure 5**).

Ranolazine and lidocaine induced distinct ECG phenotypes in WT and *Scn1b* null mice

To understand how $Na_V\beta1/\beta1B$ modulate antiarrhythmic responses at the whole heart level, we measured surface ECGs in anesthetized WT and *Scn1b* null mice before and after intraperitoneal (IP) injection of lidocaine or ranolazine (**Figure 6, Supplement Table 1**). From the raw ECG data, we quantified several parameters that describe overall heart electrical functioning, including: RR intervals, providing a measure of heart rates; P wave intervals, representing atrial conduction; PR intervals, characterizing atrial-ventricular conduction; QRS intervals, revealing ventricle conduction; and, QT and ST intervals, corresponding to ventricular repolarization.

We found that 20 mg/kg ranolazine caused QRS prolongation in both WT and *Scn1b* null mice (**Figure 6A, B**), but that P wave and PR interval prolongation only occurred in the *Scn1b* null mice (**Figure 6B**). The QT interval, but not the ST interval, was also prolonged by ranolazine in *Scn1b* null mice (**Figure 6B and Supplement Figure 3**). These results suggest that *Scn1b* deletion enhances the inhibitory effect of ranolazine on cardiac conduction. Similar to the effects observed at the single myocyte level (**Figures 4 and 5**) that the loss of *Scn1b* enhanced TB and

UDB of I_{Na} by ranolazine, loss of Navβ1/β1B in *Scn1b* null mice promotes ranolazine block, manifesting as P wave, PR, and QRS interval prolongation.

We observed that 30 mg/kg lidocaine administration increased P wave duration in both WT and *Scn1b* null mice (**Figure 6A, C).** In addition, lidocaine induced prolongation of RR, QT, and ST intervals in WT, but not *Scn1b* null mice (**Figure 6C and Supplement Figure 3**). In contrast, lidocaine increased PR and QRS intervals in *Scn1b* null mice (**Figure 6C**). Lidocaine injection, therefore, result in distinct functional effects in the two genotypes. Control experiments, in which we measured ECGs before and after injection of phosphate-buffered (PBS) solution. Comparison of baseline and post-PBS data showed that ECG parameters remained constant (**Supplement Figure 4**).

SCN1B is differentially expressed in human atria and ventricles

The observation that loss of *Scn1b* alters the ability of Class Ib antiarrhythmics to block Na_V channels in mouse heart suggest that the differential expression of *SCN1B* might play an important role in regulating antiarrhythmic drug responses in humans. To begin to explore this hypothesis, we examined mRNA expression levels of the genes (*SCN1B*, *SCN2B*, *SCN3B*, and *SCN4B*) encoding $Na_V\beta$ subunits in human heart tissue in a recently published RNA sequencing (RNAseq) library(35). These analyses revealed that, in the human heart, *SCN1B* is the most abundant of the $Na_V\beta$ subunits at the transcript level and, in addition, that *SCN1B* transcript expression is much higher in atria than in ventricles (**Figure 7A**). In contrast, the expression levels of the *SCN2B* and *SCN4B* transcripts are higher in the ventricles than in the atria (**Figure 7A**). To validate the RNAseq findings and to determine if both *SCN1B* splice variants, *SCN1BA* ($Na_v\beta1$) and *SCN1BB* ($Na_v\beta1B$), are differentially expressed in human atria and ventricles, we performed quantitative RT-PCR analyses on the same tissue samples as used in the RNAseq

analyses. These experiments revealed that the relative expression levels of the two *SCN1B* splice variants were significantly higher in the atria, compared to the ventricles (**Figure 7B**). Additional analyses revealed that, although expression of *SCN1BA* is ~100 fold higher than *SCN1BB*, the similar expression levels of the two (*SCN1BA* and *SCN1BB*) splice variants are similar in human right and left atria (RA and LA), and in human right and left ventricles (RV and LV) (**Supplement Figure 5**).

Discussion

Although class Ib antiarrhythmics have considerable therapeutic potential, they are not broadly prescribed because of proarrhythmic risks in some patients and they are ineffective in others(36, 37). Patient or disease variability in class Ib drug response suggests that there are external factors that modulate drug interactions with the channel(37). In this study, we investigated the role of Na_V channel accessory subunits $Na_V\beta1$ and $Na_V\beta3$ in regulating class Ib antiarrhythmic-mediated effects on $Na_V1.5$ channels. We demonstrated that, at a molecular level $Na_V\beta1$ or $Na_V\beta3$ subunit co-expression differentially alters the effects of lidocaine and ranolazine on the $Na_V1.5$ DIII-VSD. $Na_V\beta1$ enhances lidocaine but inhibits ranolazine modulation of the DIII-VSD. Conversely, $Na_V\beta3$ eliminates lidocaine modulation but increases the effect of ranolazine on the DIII-VSD. Differential molecular interactions between $Na_V1.5$ DIII-VSD and class Ib antiarrhythmic drugs caused by Navβ1 subunit expression in a heterologous system translated to distinct drug blockade of Na_V channels in WT vs. *Scn1b* cardiac-specific null mouse cardiomyocytes. We further demonstrate differential effects of lidocaine and ranolazine on the ECG phenotypes of WT and *Scn1b* null mice.

Navβ1 and Navβ3 subunits alter Nav1.5 channel pharmacology via the DIII-VSD

The DIII-VSD plays an important role in regulating $Na_V1.5$ channel gating. It is involved in both activation and inactivation of Na_V channels (38, 39). Recent studies showed a correlation between DIII-VSD deactivation and the slow component of recovery from inactivation, which suggests that an activated form of the DIII-VSD stabilizes inactivation(39). As Class Ib antiarrhythmics promote DIII-VSD activation, they may subsequently promote inactivation, to induce greater levels of use dependent block. We recently demonstrated that DIII-VSD activation determines $Na_V1.5$ channel blockade by mexiletine, and affects the sensitivity of LQT3 variants to this drug(18), demonstrating a clear connection between the conformation of the DIII-VSD and Class Ib drug potency.

We previously demonstrated that $Na_V\beta3$ directly modulates the DIII-VSD, while $Na_V\beta1$ does not(14). Recent channel structures suggest that $Na_V\beta1$ associates with $Na_V1.7$ and $Na_V1.4$ through the DIII-VSD, an interaction that is not conserved in $Na_V1.5$(10, 12, 13). In light of these structural and functional data, it is plausible that $Na_V\beta3$ interacts with $Na_V1.5$ through similar sites as illustrated in the $Na_V1.4$/ $Na_V1.7$-β1 complex, while $Na_V\beta1$ occupies a different site. Two distinct interaction mechanisms will result in the differential modulation of the DIII-VSD by Navβ1 and Navβ3. Here, we show that co-expression of the $Na_V\beta1$ or $Na_V\beta3$ subunit differentially modulates the ability of Class Ib antiarrhythmics to stabilize the DIII-VSD in the activated conformation, providing further evidence that, in contrast to other Na_V channel α subunits, $Na_V\beta1$ and $Na_V\beta3$ have distinct interactions with $Na_V1.5$. The effect of lidocaine on the DIII-VSD has been previously shown to regulate UDB, a critical feature of Class-Ib drugs, which renders them most potent when myocytes are being excited repeatedly during an arrhythmic event. We observed that ranolazine and lidocaine similarly affect $Na_V1.5$ α subunit-encoded channels expressed in the absence of the Navβ subunits. However, with the $Na_V\beta1$

subunit present, the lidocaine effect on the DIII-VSD was enhanced, while the ranolazine effect was blunted. Conversely, $Na_V\beta3$ enhanced ranolazine-induced DIII-VSD stabilization, while inhibiting the effect of lidocaine. The differential regulation of the DIII-VSD resulted in distinct effects on the potencies of lidocaine and ranolazine depending on which $Na_V\beta$ is present. Thus, despite the similarity of the chemical structures (**Figure 1**), the therapeutic responses to lidocaine and ranolazine are differentially modified by the co-expression of the $Na_V\beta1$ or the $Na_V\beta3$ subunit.

$Na_V\beta1$/β1B modulates Class Ib antiarrhythmic responses from molecular to the whole heart level

In *Xenopus* oocytes, with VCF and cut-open voltage clamp recordings, we demonstrated that $Na_V\beta1$ co-expression enhanced lidocaine's, but inhibited ranolazine's, effect on the DIII-VSD, which resulted in an increased lidocaine, but decreased ranolazine, block. In addition, we observed increased UDB and late I_{Na} block by lidocaine, but opposite effects with ranolazine, in WT, compared with *Scn1b* null, mouse LV myocytes. This cellular difference further led to distinct phenotypes of the *in vivo* ECG recordings in response to lidocaine and ranolazine injections. For example, in response to ranolazine injection, the P wave duration and PR interval were prolonged in the *Scn1b* null mice, but not in the WT mice. This difference in ECG parameters reflects the cellular phenotype of enhanced ranolazine block of I_{Na} in *Scn1b* null, compared with WT, LV myocytes. However, not all the ECG changes can be explained by the differences observed in myocyte I_{Na} recordings of atrial and ventricular myocytes, and they may be caused by $Na_V\beta1$-mediated effects on other regions of the myocardium, such as the sinoatrial (SA) and atrioventricular (AV) nodes(40). Alternatively, $Na_V\beta1$ may affect drug interactions with other ion channels that regulate cardiac excitation, as discussed further below.

Differential expression of Navβ1/β1B in human atria and ventricles and chamber-specific drug responses

Ranolazine was proposed as a candidate for atrial specific therapy for AF (24, 41). Studies in canine heart showed that atrial and ventricular cardiomyocytes have distinct responses to ranolazine(24). In the atria, ranolazine prolongs the action potential duration measured at 90% repolarization (APD_{90}) and effective refractory period (ERP) (24). In contrast, in the ventricle, ranolazine shortens the APD_{90}. Here, we demonstrate higher *SCN1Ba* ($Na_V\beta1$) and *SCN1Bb* ($Na_V\beta1B$) subunit mRNA expression levels in human atria, compared to ventricles. While we showed that $Na_V\beta1$ co-expression attenuates ranolazine block of I_{Na} in both *Xenopus* oocytes and mouse LV myocytes, higher levels of $Na_V\beta1$ in human atria may result in similar attenuation of the effects of ranolazine, thus contributing to decreased ranolazine blockade compared to ventricles. Notably, ranolazine is also a blocker of *KCNH2*- (HERG-) encoded repolarizing I_{Kr} channels(22). If ranolazine blockade of I_{Na} is reduced in atria, modulation of I_{Kr} may dominate, resulting in prolongation of APD specifically in atria. Thus, the heterogeneous expression of $Na_V\beta1$ may play a role in the chamber-specific ranolazine response.

Navβ subunit modulation of class Ib drug effects may underlie disease-specific drug responses

A search of the Gene Expression Omnibus (GEO) Profiles database(42) revealed that *SCN1B* is upregulated in ischemic cardiomyopathies in human heart (GEO accessions GDS651 and GDS1362(43)) and mouse heart failure models (GEO accessions GDS411, GDS427(44), and GDS3660(45)) (**Supplement Figure 6**). These data suggest that the expression of $Na_V\beta$ subunits can be altered in disease remodeling of the cardiac tissue. Since late I_{Na} was found to be increased in failing heart, class Ib drugs have become potential therapeutic approaches in

targeting heart failure related arrhythmias(46). As we have demonstrated that Navβ can differentially modulate class Ib effects, upregulation of $Na_V\beta1$ in failing tissue may alter the patient response to Na_V channel-targeting antiarrhythmic therapies.

Differential effects of Navβ subunits on lidocaine and ranolazine interactions reflect distinct molecular drug-pore interactions

Previous work postulated that both lidocaine and ranolazine bind to common residues in the $Na_V1.5$ channel pore (20, 31). However, we observed that lidocaine modulates both the DIII- and DIV-VSDs of $Na_V1.5$, whereas ranolazine only affects the DIII-VSD when the Nav1.5 is expressed without Navβ subunits, suggesting that these compounds may present in different orientations in the channel pore. Recent molecular dynamics simulations shed light on the detailed binding conformations of lidocaine and ranolazine within the $Na_V1.5$ channel(47). Interestingly, these studies revealed that two lidocaine molecules can bind to the pore concurrently, one to the F1760 site and the other to the central pore(47). In contrast, ranolazine binds to the F1760 residue and possesses a more flexible linear structure, allowing it to interact with a larger area ranging from the fenestration to the selectivity filter(47). Moreover, ranolazine has a pK_a of 7.2(48), while lidocaine has a pK_a of 7.9(49). At physiological pH, therefore, a higher percentage of ranolazine molecules are expected to be uncharged compared to lidocaine. This difference will determine the relative percentages of the drug molecules entering in the hydrophobic pathway through the fenestration versus the hydrophilic pathway via the intracellular gate. The presence of Navβ1 or Navβ3 modulates DIII-VSD and DIV-VSD dynamics, which can allosterically affect the conformation of the pore and fenestrations. We demonstrated that Navβ1/β3's modulation of ranolazine block is not entirely dependent on the main local anesthetic binding site, F1760, suggesting the changes in the DIII-VSD conformation

due to Navβ modulation are essential for determining drug accessibility to the pore, independent of binding. In contrast, eliminating the F1760 binding site abolished the effects of Navβ1/β3 coexpression on lidocaine block, further suggesting that lidocaine acts through mechanisms distinct from those of ranolazine. Because lidocaine and ranolazine have different stoichiometries, orientations within the pore, and entrance pathways, it is plausible that changing channel VSD and pore conformations in the presence of $Na_V\beta$ subunits can result in opposite effects on DIII-VSD interactions with these drugs.

Navβ subunit modulation of antiarrhythmic drug outcome beyond Na_V channels

Aside from Na_V channels, $Na_V\beta$ subunits have been shown to modulate expression and gating of various potassium channels, including the voltage-gated K_V 4.3 and the inward-rectifying K_{ir} 2.1 channels, resulting in modifications of two essential cardiac currents, the fast transient outward K^+ current ($I_{to,f}$) and the inwardly rectifier current (I_{K1})(50–52). Although unexplored to date, it also seems highly likely that the presence of $Na_V\beta$ subunits can affect K_V and K_{ir} channel pharmacology as well. Here, we showed that, while single cardiac-specific *Scn1b* null LV myocytes display attenuated inhibition of I_{Na} by lidocaine, compared with WT cells, enhanced PR and QRS interval prolongation is observed in *Scn1b* null animals with lidocaine, suggesting contributions from other cardiac ionic currents.

Limitations

To assess the drug effects on VSD dynamics, we conducted the VCF experiments in *Xenopus* oocytes. As this is a heterologous expression system and the experiments were performed at 19 °C, extrapolating the results to mammalian physiology can be difficult. However, we observed consistent drug-mediated modulatory effects in oocytes and in mouse LV myocytes, observations

which support the hypothesis that the molecular mechanisms we identified with VCF are operative in mammalian systems.

We were only able to show that the expression of *SCN1B* is enriched in atria compared to ventricles in human heart at the transcript level. Although we attempted to examine protein expression levels directly, none of the available anti-$Na_V\beta1$ antibodies detect $Na_V\beta1$ proteins in mouse or human cardiac tissues. Since it is currently not possible to perform gene-editing or to use small interfering RNA-mediated knockdown strategies in native human myocytes, we were not able to explore the functional effects of $Na_V\beta1$ on class Ib drugs in human myocytes directly.

Conclusions

In summary, we have demonstrated roles for non-covalently linked $Na_V\beta$ subunits in regulating anti-arrhythmic drug effects from molecular interactions to whole heart phenotypes. Our results elucidate the differential regulation of $Na_V1.5$ channels by two Class-Ib agents, lidocaine and ranolazine, by $Na_V\beta1$ and $Na_V\beta3$ subunits. The unique expression profile of $Na_V\beta$ subunits in human heart suggests chamber-dependent responses to these two compounds. Our findings provide crucial insights into strategies for improving the clinical outcomes of patients treated with Class-Ib agents for different forms of arrhythmias. Moreover, $Na_V\beta1$ expression is upregulated in heart failure and it remains unexplored whether $Na_V\beta$ subunit expression is affected in other heart pathologies. This knowledge will be highly valuable in establishing disease-specific approaches to personalize arrhythmia treatment with lidocaine and ranolazine as known changes in β-subunit expression will have predictable effects on therapeutic outcomes.

Methods and Materials

Experimental Animals

Adult (8-15 week old) male and female, wild-type (WT) and cardiac specific *Scn1b* null C57BL/6J mice were used in the experiments here. Cardiac specific *Scn1b* null mice were generated by crossing *Scn1b*^{flox} mice[27] with *B6.FVBTg(Myh6-cre)2182Mds/J* mice (Jackson Laboratories), which expresses Cre recombinase driven by the α-myosin heavy chain promoter. Mice were genotyped by PCR analyses of genomic (tail) DNA using primers targeting sequences external to the loxP sites, as well primers targeting *Cre* recombinase, as previously described[27]. Because of the breeding strategy required to generate cardiac specific *Scn1b* null C57BL/6J mice, WT littermates were not generated. The WT mice used in the experiments presented here, therefore, were not littermate controls; rather they were WT C57BL/6J from our colony. Additional control experiments, however, were conducted on *Scn1b*^{flox} and *B6.FVBTg(Myh6-cre)2182Mds/J* mice, which were determined to be indistinguishable electrophysiologically from WT C57BL/6J animals. Xenopus oocyte harvests were performed as described previously(53).

Cut-open Voltage Clamp Fluorometry:

VCF experiments were conducted using four previously developed $Na_V1.5$ channel constructs (DI: V215C, DII: S805C, DIII: M1296C, DIV: S1618C)(53). Capped mRNAs were synthesized with the mMESSAGE mMACHINE T7 transcription Kit (Life Technologies) from the linearized pMAX vectors. VCF construct mRNA was injected alone or co-injected with *SCN1B* or *SCN3B* mRNA into *Xenopus* oocytes as previously described(14). VCF experiments were performed 4-6 days after injection. The recording set-up and labeling protocol used were described previously(14, 53–55). Lidocaine hydrochloride and ranolazine dihydrochloride were dissolved

in extracellular recording solution, then further diluted to 10 mmol/L and 4 mmol/L, respectively. Both drugs were manually perfused into the extracellular solution chamber in the cut-open voltage clamp setup. Fluorescence signals and currents were analyzed as previously described (18). $V_{1/2}$ values reported were quantified from the Boltzmann function fit ($y=1/(1+\exp((V-V_{1/2})/k)$). As the DIII F-V curve, especially under drug treatment conditions, did not saturate at the lowest voltage recorded (-160 mV), the fit was performed fixing 0 at -200 mV. Due to the lack of saturation at the most negative potentials measured, the estimated $V_{1/2}$ for DIII F-V is likely to be higher than the actual $V_{1/2}$ value.

ECG recordings:

Surface electrocardiographic (ECG) recordings were obtained as previously described from mice anaesthetized by intraperitoneal injection (IP) of Avertin (0.25 mg/kg,; Sigma, St Louis)(56). Baseline ECGs were recorded, and animals were weighed. For injections, drugs were dissolved in (250 µl) phosphate buffered saline (PBS). Lidocaine or ranolazine was then injected at a dosage of 30 mg/kg or 20 mg/kg, respectively. Different animals were used for lidocaine or ranolazine injections. Between recordings, mice were kept on a heating pad maintained at 37 ± 0.5 °C. Post-injection ECGs were recorded at 5 min, 10 min, 15 min, 20 min, and 30 min. Peak responses were observed at 10 min, which was subsequently selected as the time point for ECG analysis.

RR, PR and QT intervals, as well as P and QRS durations, were measured and compiled using Clampfit 10.3 (Molecular Devices) and GraphPad (Prism). Note that QT intervals shown in figures were not corrected as several recent studies have shown that QT intervals in anesthetized mice do not vary with heart rate (57, 58). Similar differences were revealed, however, when corrected QT intervals were compared (Supplemental Table 1).

Isolation of adult mouse cardiomyocytes:

Myocytes were isolated from adult (8 to 12 week) WT or *Scn1b null* mice as previously described(59). Briefly, hearts were isolated and perfused retrogradely through the aorta with a Ca^{2+}-free Eagle's balanced salt solution containing (0.8mg/ml) Type II collagenase (Worthington). After perfusion, the left ventricular (LV) free wall was dissected and minced. The tissue pieces were then triturated to provide individual LV myocytes. Dispersed cells were then filtered and resuspended in Medium199 (Gibco), plated on laminin (Sigma) coated glass coverslips and maintained in a 95% air/5% CO_2 incubator at 37°C.

Whole-cell Na_V current (I_{Na}) recordings were obtained from isolated LV myocytes at room temperature (22-24 °C) within 5-6 hours of isolation using a Dagan 3900A (Dagan) amplifier, interfaced to a Digidata 1332A A/D converter (Axon) using pClamp 10.2 (Axon). Recording pipettes contained (in $mmolL^{-1}$): 120 glutamic acid, 120 CsOH, 10 HEPES, 0.33 $MgCl_2$, 20 tetraethylammonium chloride (TEA-Cl), 4 Mg-ATP, 5 glucose and 5 EGTA (pH adjusted to 7.3 with CsOH; pipette resistances were 1.5-3.0 MΩ. The bath solution contained (in mM): 20 mM NaCl, 110 mM TEACl, 4 KCl, 2 $MgCl_2$, 1 $CaCl_2$, 10 HEPES and 10 glucose (pH 7.4; 300 mOsm). Electrophysiological data were acquired at 10-20 KHz and signals were low pass filtered at 5 kHz before digitization and storage. After the formation of a giga-seal (>1 GΩ) and establishment of the whole-cell configuration, brief (10 ms) ± 10 mV voltage steps from a holding potential (HP) of -70 mV were presented to allow measurements of whole-cell membrane capacitances (C_m), input resistances (R_{in}) and series resistances (R_s). In each cell, C_m and R_s were compensated electronically by ~85%; voltage errors resulting from uncompensated series resistances were <2 mV and were not corrected. Leak currents were always <50 pA and were not corrected. Whole-

cell I_{Na} were evoked in response to 40 ms voltage steps to potentials between -60 to + 40 mV from a HP of -100 mV in 10 mV increments at 15s intervals.

Electrophysiological data were compiled and analyzed using Clampfit 10.3 (Molecular Devices) and GraphPad (Prism).

Quantitative Reverse Transcription PCR:

Total RNA (2 µg) isolated from individual matched (n = 6) human RA, LA, RV and LV tissue samples was reverse transcribed into cDNA with a High Capacity cDNA kit (Applied Biosystems). Transcript analysis was conducted with SYBR Green (Applied Biosystems) using a 7900HT Fast Real-Time PCR system (Applied Biosystems). Data were analyzed using the threshold cycle (C_T) relative quantification method using the glyceraldehyde 3-phosphate dehydrogenase (*GAPDH*) and hypoxanthine guanine phosphoribosyl transferase I (*HPRT*) genes as endogenous controls.

Statistics:

Results are presented as means ± standard error of the means (SEM). The numbers of animals and the numbers of cells used in each experiment are provided in the figure legends. Comparisons of differences between WT and *Scn1b* null cells/animals under control conditions and before and after drug treatments were performed using a paired two-tailed Student's *t* test (Microsoft Excel). In comparisons more than 2 groups, one-way ANOVA was used, followed by multiple comparisons. The p values shown were corrected for multiple hypothesis testing using the Dunnett correction method.

Study approval

All animals were handled in accordance with the NIH Guide for the Care and Use of Laboratory Animals, and all experimental protocols were approved by the Washington University Institutional Animal Care and Use Committee (IACUC).

Author contributions:

WZ contributed to designing studies, conducting experiments, acquiring data, analyzing data, and writing the manuscript. WW, PA, and RLM contributed to conducting experiments and acquiring data. LLI contributed to providing experimental animals and editing manuscript. JMN. and JRS contributed to designing studies and editing manuscript.

Acknowledgements and Sources of Funding:

Human cardiac tissue samples were provided by the Translational Cardiovascular Biobank and Repository (TCBR), supported by the Washington University Institute for Clinical and Translational Sciences (ICTS), recipient of a Clinical and Translational Sciences Award (UL1 RR024992) from the NIH National Center for Research Resources.

Financial support was provided by the American Heart Association (AHA) (Predoctoral Fellowship 15PRE25080073 WZ), NIH National Heart, Lung and Blood Institute (R01 HL136553 JRS), NIH National Heart, Lung and Blood Institute (R01 HL-034161 and R01 HL-142520 to JMN). These funding sources were involved in study design, data collection, data analyses, data interpretation, manuscript preparation or the decision to submit this article for consideration for publication.

Disclosures:

The authors have declared that no conflicts of interest exist.

References:

1. Zipes DP, Jalife J. *Cardiac Electrophysiology: From Cell to Bedside: Sixth Edition*. 2013:

2. Gellens ME et al. Primary structure and functional expression of the human cardiac tetrodotoxin-insensitive voltage-dependent sodium channel.. *Proc. Natl. Acad. Sci. U. S. A.* 1992;89:554–558.

3. Abriel H. Cardiac sodium channel Nav1.5 and interacting proteins: Physiology and pathophysiology. *J. Mol. Cell. Cardiol.* 2010;48(1):2–11.

4. Calhoun JD, Isom LL. The Role of Non-pore-Forming β Subunits in Physiology and Pathophysiology of Voltage-Gated Sodium Channels [Internet]. In: *Voltage Gated Sodium Channels*. 2014:51–89

5. Patino GA et al. Voltage-Gated Na+ Channel 1B: A Secreted Cell Adhesion Molecule Involved in Human Epilepsy. *J. Neurosci.* 2011;31:14577–14591.

6. Rehm HL et al. ClinGen — The Clinical Genome Resource [Internet]. *N. Engl. J. Med.* 2015;372(23):2235–2242.

7. Gray B et al. Lack of genotype-phenotype correlation in Brugada Syndrome and Sudden Arrhythmic Death Syndrome families with reported pathogenic SCN1B variants.. *Hear. Rhythm* 2018;15(7):1051–1057.

8. Yuan L et al. Investigations of the Navβ1b sodium channel subunit in human ventricle; functional characterization of the H162P Brugada syndrome mutant. [Internet]. *Am. J. Physiol. Heart Circ. Physiol.* 2014;306(8):H1204-12.

9. Isom LL et al. Primary structure and functional expression of the beta 1 subunit of the rat brain sodium channel.. *Science* 1992;256:839–842.

10. Yan Z et al. Structure of the Nav1.4-β1 Complex from Electric Eel. *Cell* [published online ahead of print: 2017]; doi:10.1016/j.cell.2017.06.039

11. Pan X et al. Structure of the human voltage-gated sodium channel Nav1.4 in complex with β1 [Internet]. *Science (80-.).* 2018;362(6412):eaau2486.

12. Shen H, Liu D, Wu K, Lei J, Yan N. Structures of human Nav1.7 channel in complex with auxiliary subunits and animal toxins [Internet]. *Science (80-.).* 2019;363(6433):1303 LP – 1308.

13. Jiang D et al. Structure of the Cardiac Sodium Channel [Internet]. *Cell* [published online ahead of print: January 4, 2020]; doi:10.1016/j.cell.2019.11.041

14. Zhu W et al. Mechanisms of noncovalent β subunit regulation of Na_V channel gating [Internet]. *J. Gen. Physiol.* 2017;149(8):813–831.

15. Salvage SC et al. Gating control of the cardiac sodium channel Nav1.5 by its β3-subunit involves distinct roles for a transmembrane glutamic acid and the extracellular domain [Internet]. *J. Biol. Chem.* [published online ahead of print: October 28, 2019]; doi:10.1074/jbc.RA119.010283

16. Muroi Y, Chanda B. Local anesthetics disrupt energetic coupling between the voltage-sensing segments of a sodium channel. [Internet]. *J. Gen. Physiol.* 2009;133(1):1–15.

17. Sheets MF, Hanck DA. Outward stabilization of the S4 segments in domains III and IV enhances lidocaine block of sodium channels [Internet]. *J. Physiol.* 2007;582(1):317–334.

18. Zhu W et al. Predicting patient response to the antiarrhythmic mexiletine based on genetic variation: Personalized medicine for long QT syndrome. *Circ. Res.* [published online ahead of print: 2019]; doi:10.1161/CIRCRESAHA.118.314050

19. Moreno JD, Zhu W, Mangold K, Chung W, Silva JR. A Molecularly Detailed NaV1.5 Model Reveals a New Class I Antiarrhythmic Target. *JACC Basic to Transl. Sci.* [published online ahead of print: 2019]; doi:10.1016/j.jacbts.2019.06.002

20. Ragsdale DS, McPhee JC, Scheuer T, Catterall WA. Common molecular determinants of local anesthetic, antiarrhythmic, and anticonvulsant block of voltage-gated Na+ channels [Internet]. *Proc. Natl. Acad. Sci. U. S. A.* 1996;93:9270–9275.

21. Gianelly R, von der Groeben JO, Spivack AP, Harrison DC. Effect of Lidocaine on Ventricular Arrhythmias in Patients with Coronary Heart Disease [Internet]. *N. Engl. J. Med.* 1967;277(23):1215–1219.

22. Antzelevitch C, Burashnikov A, Sicouri S, Belardinelli L. Electrophysiologic basis for the antiarrhythmic actions of ranolazine. *Hear. Rhythm* 2011; doi:10.1016/j.hrthm.2011.03.045

23. Guerra F, Romandini A, Barbarossa A, Belardinelli L, Capucci A. Ranolazine for rhythm control in atrial fibrillation: A systematic review and meta-analysis. *Int. J. Cardiol.* [published online ahead of print: 2017]; doi:10.1016/j.ijcard.2016.11.103

24. Burashnikov A, Di Diego JM, Zygmunt AC, Belardinelli L, Antzelevitch C. Atrium-selective sodium channel block as a strategy for suppression of atrial fibrillation: Differences in sodium channel inactivation between atria and ventricles and the role of ranolazine [Internet]. *Circulation* 2007;116(13):1449–1457.

25. Antzelevitch C, Burashnikov A, Sicouri S, Belardinelli L. Electrophysiologic basis for the antiarrhythmic actions of ranolazine. *Hear. Rhythm* [published online ahead of print: 2011]; doi:10.1016/j.hrthm.2011.03.045

26. Ramirez RJ et al. Mechanisms by Which Ranolazine Terminates Paroxysmal but Not Persistent Atrial Fibrillation. *Circ. Arrhythm. Electrophysiol.* 2019;12(10):e005557.

27. Zareba W et al. Ranolazine in High-Risk Patients With Implanted Cardioverter-Defibrillators: The RAID Trial. *J. Am. Coll. Cardiol.* [published online ahead of print: 2018]; doi:10.1016/j.jacc.2018.04.086

28. Lin X et al. Scn1b deletion leads to increased tetrodotoxin-sensitive sodium current, altered intracellular calcium homeostasis and arrhythmias in murine hearts. [Internet]. *J. Physiol.* 2014;00:1–19.

29. Arcisio-Miranda M, Muroi Y, Chowdhury S, Chanda B. Molecular mechanism of allosteric modification of voltage-dependent sodium channels by local anesthetics.. *J. Gen. Physiol.* 2010;136(5):541–554.

30. Hanck DA et al. Using lidocaine and benzocaine to link sodium channel molecular conformations to state-dependent antiarrhythmic drug affinity. *Circ. Res.* 2009;105(5):492–499.

31. Ragsdale DS, McPhee JC, Scheuer T, Catterall WA. Molecular determinants of state-dependent block of Na+ channels by local anesthetics. [Internet]. *Science* 1994;265(5179):1724–8.

32. Hille B. Local anesthetics: hydrophilic and hydrophobic pathways for the drug-receptor reaction. [Internet]. *J. Gen. Physiol.* 1977;69(4):497–515.

33. Lopez-Santiago LF et al. Sodium channel Scn1b null mice exhibit prolonged QT and RR intervals. [Internet]. *J. Mol. Cell. Cardiol.* 2007;43(5):636–47.

34. Zhu W, Li T, Silva JR, Chen J. Conservation and divergence in NaChBac and NaV1.7 pharmacology reveals novel drug interaction mechanisms. *Sci. Rep.* [published online ahead of print: 2020]; doi:10.1038/s41598-020-67761-5

35. Johnson EK, Matkovich SJ, Nerbonne JM. Regional Differences in mRNA and lncRNA Expression Profiles in Non-Failing Human Atria and Ventricles. *Sci. Rep.* [published online ahead of print: 2018]; doi:10.1038/s41598-018-32154-2

36. Zimetbaum P. Antiarrhythmic drug therapy for atrial fibrillation. *Circulation* [published online ahead of print: 2012]; doi:10.1161/CIRCULATIONAHA.111.019927

37. Mazzanti A et al. Gene-specific therapy with mexiletine reduces arrhythmic events in patients with long QT syndrome type 3 [Internet]. *J. Am. Coll. Cardiol.* 2016;67(9):1053–1058.

38. Cha A, Peter C. R, Alfred L. G, Esther F, Francisco B. Voltage sensors in domains III and IV, but not I and II, are immobilized by Na+ channel fast inactivation. *Neuron* 1999;22(1):73–87.

39. Hsu EJ et al. Regulation of Na(+) channel inactivation by the DIII and DIV voltage-sensing domains. [Internet]. *J. Gen. Physiol.* 2017;149(3):389–403.

40. Domínguez JN, Navarro F, Franco D, Thompson RP, Aránega AE. Temporal and spatial expression pattern of beta1 sodium channel subunit during heart development. [Internet]. *Cardiovasc. Res.* 2005;65(4):842–50.

41. Zygmunt a. C et al. Mechanisms of atrial-selective block of Na+ channels by ranolazine: I.

Experimental analysis of the use-dependent block. *AJP Hear. Circ. Physiol.* 2011;301(4):H1606–H1614.

42. Barrett T et al. NCBI GEO: Archive for functional genomics data sets - Update. *Nucleic Acids Res.* [published online ahead of print: 2013]; doi:10.1093/nar/gks1193

43. Kittleson MM et al. Gene expression analysis of ischemic and nonischemic cardiomyopathy: Shared and distinct genes in the development of heart failure. *Physiol. Genomics* [published online ahead of print: 2005]; doi:10.1152/physiolgenomics.00255.2004

44. Blaxall BC, Spang R, Rockman HA, Koch WJ. Differential myocardial gene expression in the development and rescue of murine heart failure. *Physiol. Genomics* [published online ahead of print: 2004]; doi:10.1152/physiolgenomics.00087.2003

45. Wang T et al. Particulate matter induces cardiac arrhythmias via dysregulation of carotid body sensitivity and cardiac sodium channels. *Am. J. Respir. Cell Mol. Biol.* [published online ahead of print: 2012]; doi:10.1165/rcmb.2011-0213OC

46. Horvath B, Bers DM. The late sodium current in heart failure: pathophysiology and clinical relevance. *ESC Hear. Fail.* 2014; doi:10.1002/ehf2.12003

47. Nguyen PT, DeMarco KR, Vorobyov I, Clancy CE, Yarov-Yarovoy V. Structural basis for antiarrhythmic drug interactions with the human cardiac sodium channel. *Proc. Natl. Acad. Sci. U. S. A.* [published online ahead of print: 2019]; doi:10.1073/pnas.1817446116

48. Peters CH, Sokolov S, Rajamani S, Ruben PC. Effects of the antianginal drug, ranolazine, on the brain sodium channel NaV1.2 and its modulation by extracellular protons. *Br. J. Pharmacol.* [published online ahead of print: 2013]; doi:10.1111/bph.12150

49. Liu H, Atkins J, Kass RS. Common molecular determinants of flecainide and lidocaine block of heart Na+ channels: Evidence from experiments with neutral and quaternary flecainide analogues. *J. Gen. Physiol.* [published online ahead of print: 2003]; doi:10.1085/jgp.20028723

50. Deschênes I, Armoundas AA, Jones SP, Tomaselli GF. Post-transcriptional gene silencing of KChIP2 and Navβ1 in neonatal rat cardiac myocytes reveals a functional association between Na and Ito currents. *J. Mol. Cell. Cardiol.* [published online ahead of print: 2008]; doi:10.1016/j.yjmcc.2008.05.001

51. Deschênes I, Tomaselli GF. Modulation of Kv4.3 current by accessory subunits. *FEBS Lett.* [published online ahead of print: 2002]; doi:10.1016/S0014-5793(02)03296-9

52. Edokobi N, Isom LL. Voltage-Gated Sodium Channel β1/β1B Subunits Regulate Cardiac Physiology and Pathophysiology [Internet]. *Front. Physiol.* 2018;9:351.

53. Varga Z et al. Direct Measurement of Cardiac Na^+ Channel Conformations Reveals Molecular Pathologies of Inherited Mutations [Internet]. *Circ. Arrhythmia Electrophysiol.* 2015;CIRCEP.115.003155.

54. Rudokas MW, Varga Z, Schubert AR, Asaro AB, Silva JR. The Xenopus Oocyte Cut-open Vaseline Gap Voltage-clamp Technique With Fluorometry [Internet]. *J. Vis. Exp.* 2014;(85):1–11.

55. Zhu W, Varga Z, Silva JR. Molecular motions that shape the cardiac action potential : Insights from voltage clamp fl uorometry [Internet]. *Prog. Biophys. Mol. Biol.* 2016;1–15.

56. Marionneau C et al. Distinct cellular and molecular mechanisms underlie functional remodeling of repolarizing K+ currents with left ventricular hypertrophy. *Circ. Res.* [published

online ahead of print: 2008]; doi:10.1161/CIRCRESAHA.107.170050

57. Speerschneider T, Thomsen MB. Physiology and analysis of the electrocardiographic T wave in mice [Internet]. *Acta Physiol.* 2013;209(4):262–271.

58. Roussel J et al. The Complex QT/RR Relationship in Mice [Internet]. *Sci. Rep.* 2016;6(1):25388.

59. Brunet S et al. Heterogeneous expression of repolarizing, voltage-gated K+ currents in adult mouse ventricles. *J. Physiol.* [published online ahead of print: 2004]; doi:10.1113/jphysiol.2004.063347

Figure 1: Class Ib antiarrhythmics, lidocaine and ranolazine, alter Nav1.5 VSD conformations.

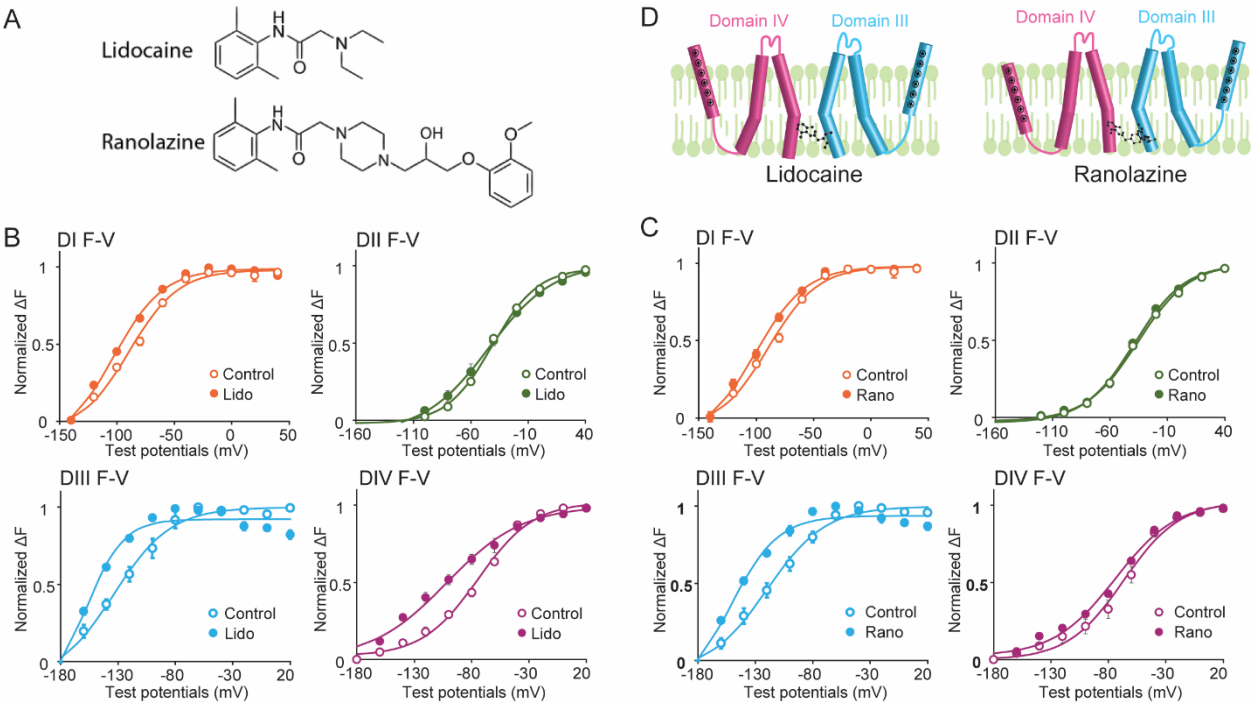

A. Chemical structures of lidocaine and ranolazine.

B. Voltage dependence of the steady-state fluorescence (F-V curves) from the four domains (DI-V215C, DII-S805C, DIII-M1296C, DIV-S1618C) of Nav1.5 before and after 10 mM lidocaine. Lidocaine was used at 10 mM to produce a robust tonic block (TB). In the presence of lidocaine, fluorescence was measured when TB reached >70%. Lidocaine induced a hyperpolarizing shift in both the DIII and DIV F-V curves.

C. F-V curves from the four domains of Nav1.5 before and after 4 mM ranolazine. Similar to the lidocaine experiment (B), in the presence of ranolazine, the fluorescence was measured when TB reached >70%. Ranolazine caused a hyperpolarizing shift in the DIII, but not in the DIV F-V curve.

D. Schematic showing effects of lidocaine and ranolazine on the DIII- and DIV-VSDs; note that each VSD is represented by a single S4 segment for clarity. Lidocaine caused both the

DIII and the DIV VSDs to stabilize in the activated conformation, whereas ranolazine only stabilized the DIII-VSD in the activated position. Each data set represents mean ± SEM values from 4-6 cells.

Figure 2: Co-expression with Navβ1 or Navβ3 differentially modulates the effect of lidocaine and ranolazine on the DIII-VSD

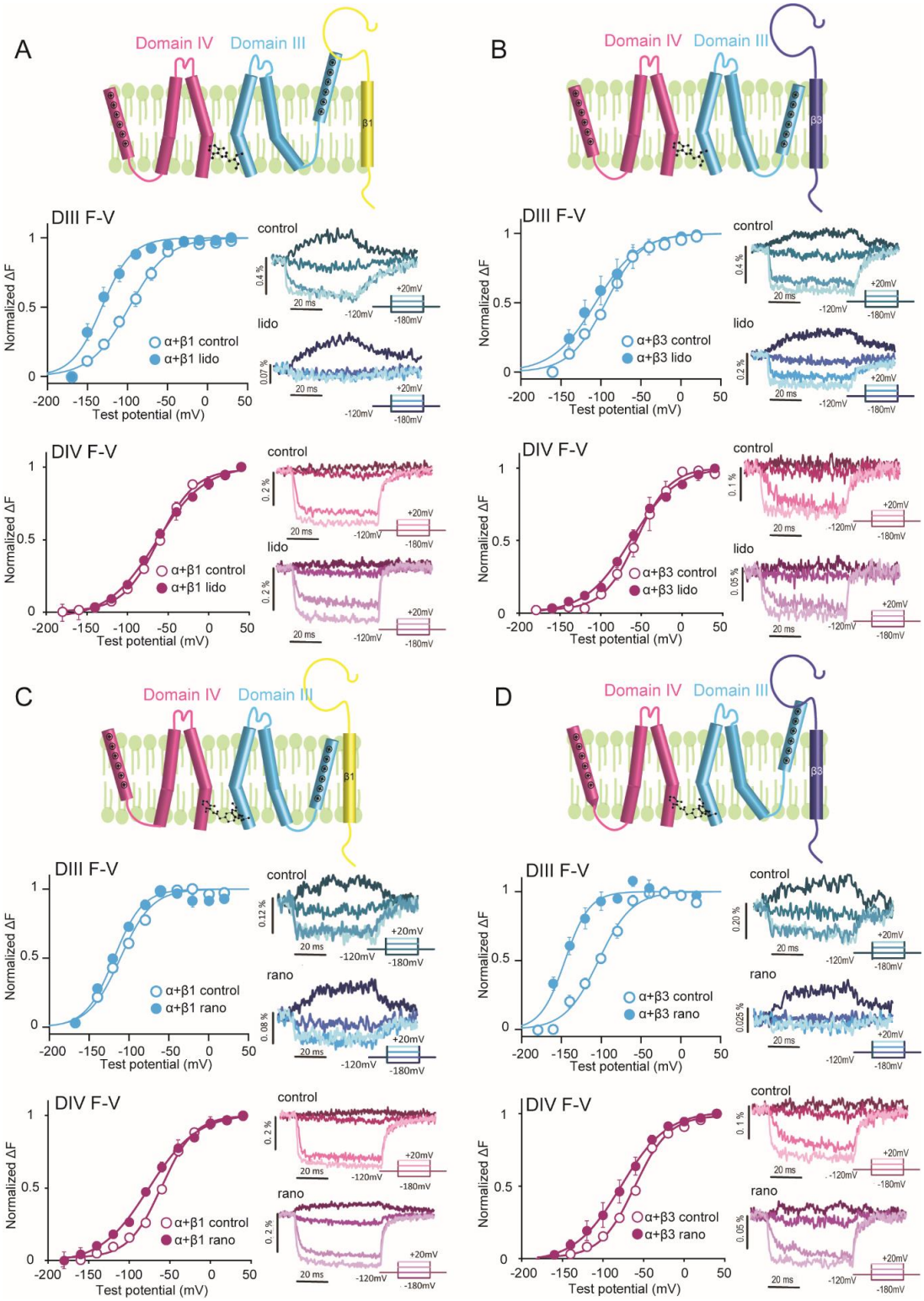

A. In the presence of $Na_V\beta1$, the hyperpolarizing shift in the DIII F-V curve produced by lidocaine was enhanced compared to the Nav1.5 α subunit expressed alone. In marked contrast, the DIV F-V curve was not affected by lidocaine with $Na_V\beta1$ present.

B. In contrast with $Na_V\beta1$ (A), the hyperpolarized shift in the DIII F-V curve induced by lidocaine is eliminated when $Na_V\beta3$ was co-expressed. Similar to $Na_V\beta1$, however, the DIV F-V curve was minimally affected by lidocaine.

C. In the presence of $Na_V\beta1$, the effect of ranolazine on the DIII F-V curve was eliminated, whereas the DIV F-V was slightly hyperpolarized.

D. In contrast with $Na_V\beta1$ (C), the hyperpolarized shift in the DIII F-V curve caused by ranolazine is enhanced when $Na_V\beta3$ was co-expressed. In the presence of $Na_V\beta3$, ranolazine also caused a small hyperpolarizing shift in the DIV F-V curve.

Each data set represents mean ± SEM values from 4-6 cells.

Figure 3: Altering the key local anesthetics (LA)' binding site F1760 did not completely abolish Na$_V$β1/β3 modulations of ranolazine block.

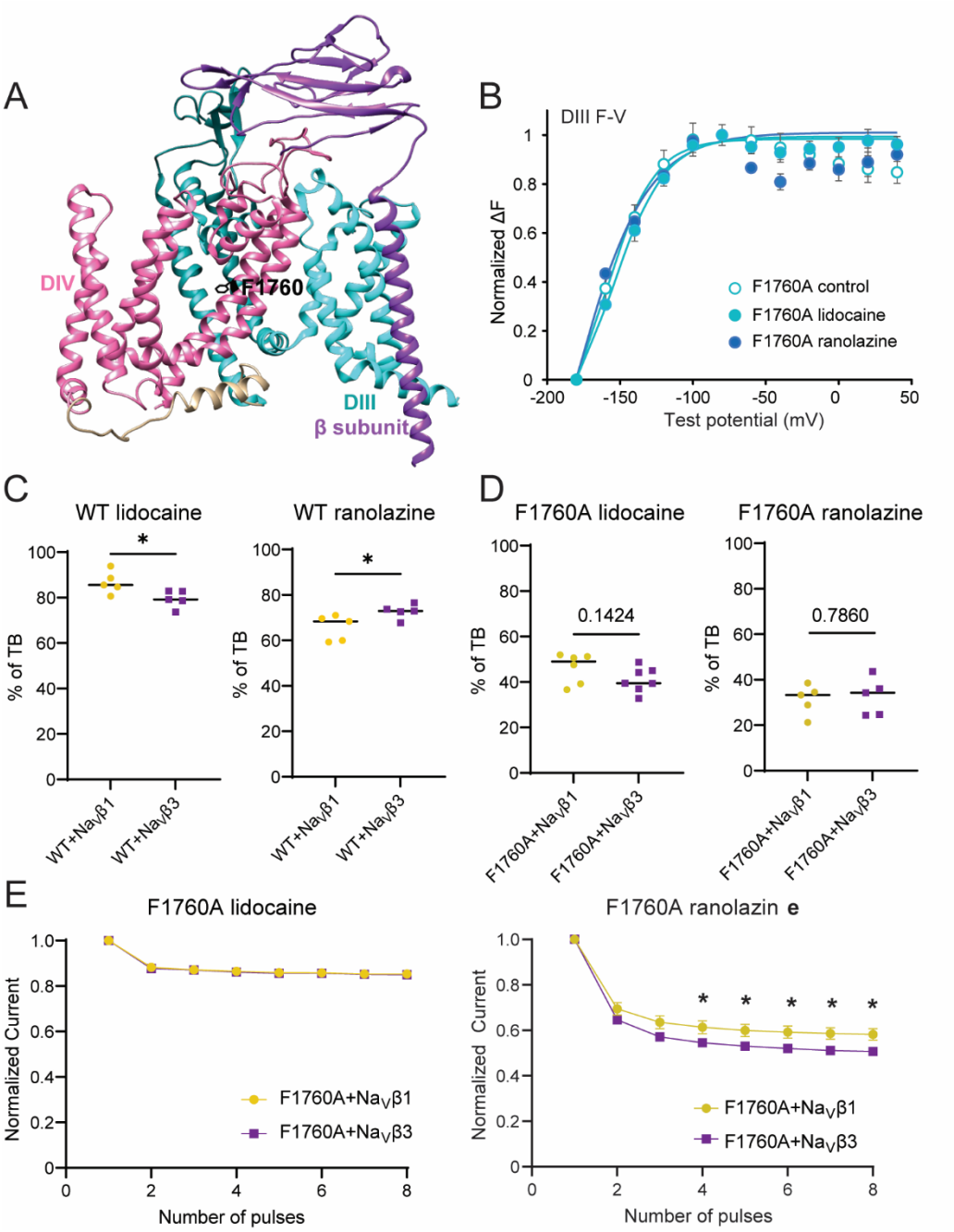

A. cryo-EM structure of human Na$_V$1.4(11) (PDB: 6AGF) showing the relative locations of the F1760 residue, DIII, DIV, and Na$_V$β1.

B. Mutating the main LA binding residue F1760 to alanine (A) greatly reduced the hyperpolarizing shift in the DIII-VSD upon 10 mM lidocaine, as well as 4 mM ranolazine, that were observed in the WT channel (Figs 1 and 2).

C. Percentage of TB induced by 10 mM lidocaine and 4 mM ranolazine in the WT channel. The presence of $Na_V\beta3$ reduced lidocaine TB, but enhanced ranolazine TB, compared to the α-$Na_V\beta1$ complex.

D. Percentage of TB induced by 10 mM lidocaine and 4 mM ranolazine in the F1760A channel. In contrast to WT, $Na_V\beta1$ and $Na_V\beta3$ no longer exert a significant effect on lidocaine and ranolazine TB.

E. UDB by lidocaine and ranolazine in F1760A channel co-expressed with $Na_V\beta1$ or $Na_V\beta3$. There is no change in lidocaine UDB comparing co-expression with $Na_V\beta1$ and $Na_V\beta3$. However, the presence of $Na_V\beta1$ caused a reduced ranolazine UDB compared to $Na_V\beta3$, a phenomenon that is similar to the $Na_V\beta1$'s effects on the WT channel.

Each data set represents mean ± SEM values from 3-6 cells. Unpaired two-tailed Student's t-test was used to test significance in C-E. * represents p-value < 0.05.

Figure 4: I_{Na} gating is similar in *Scn1b* null and WT mouse LV myocytes.

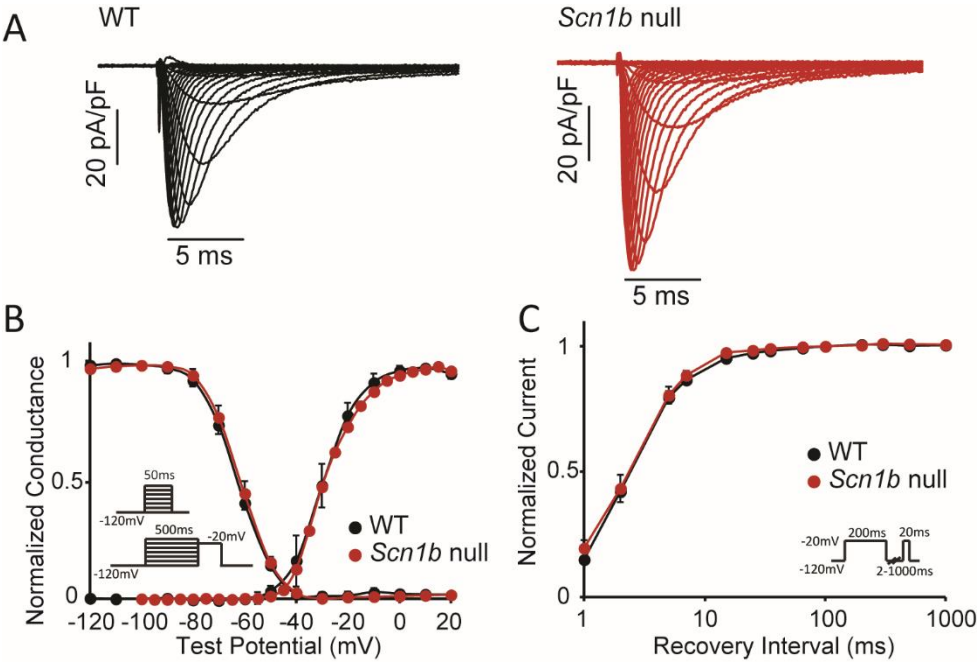

A. Representative recordings of I_{Na} in WT and *Scn1b* null mouse LV myocytes reveal similar kinetics of activation and inactivation. However, the average peak current density was slightly (~28%) higher in *Scn1b* null, compared to WT.

B. Loss of Navβ1 in *Scn1b* null mouse LV myocytes did not affect the voltage-dependences of I_{Na} activation or steady-state inactivation.

C. Loss of Navβ1 in *Scn1b* null mouse LV myocytes also did not affect the time course of I_{Na} recovery from inactivation.

Each data set represents mean ± SEM values from 6-9 cells.

Figure 5: *Scn1b* null LV myocytes show reduced lidocaine, but enhanced ranolazine, responses.

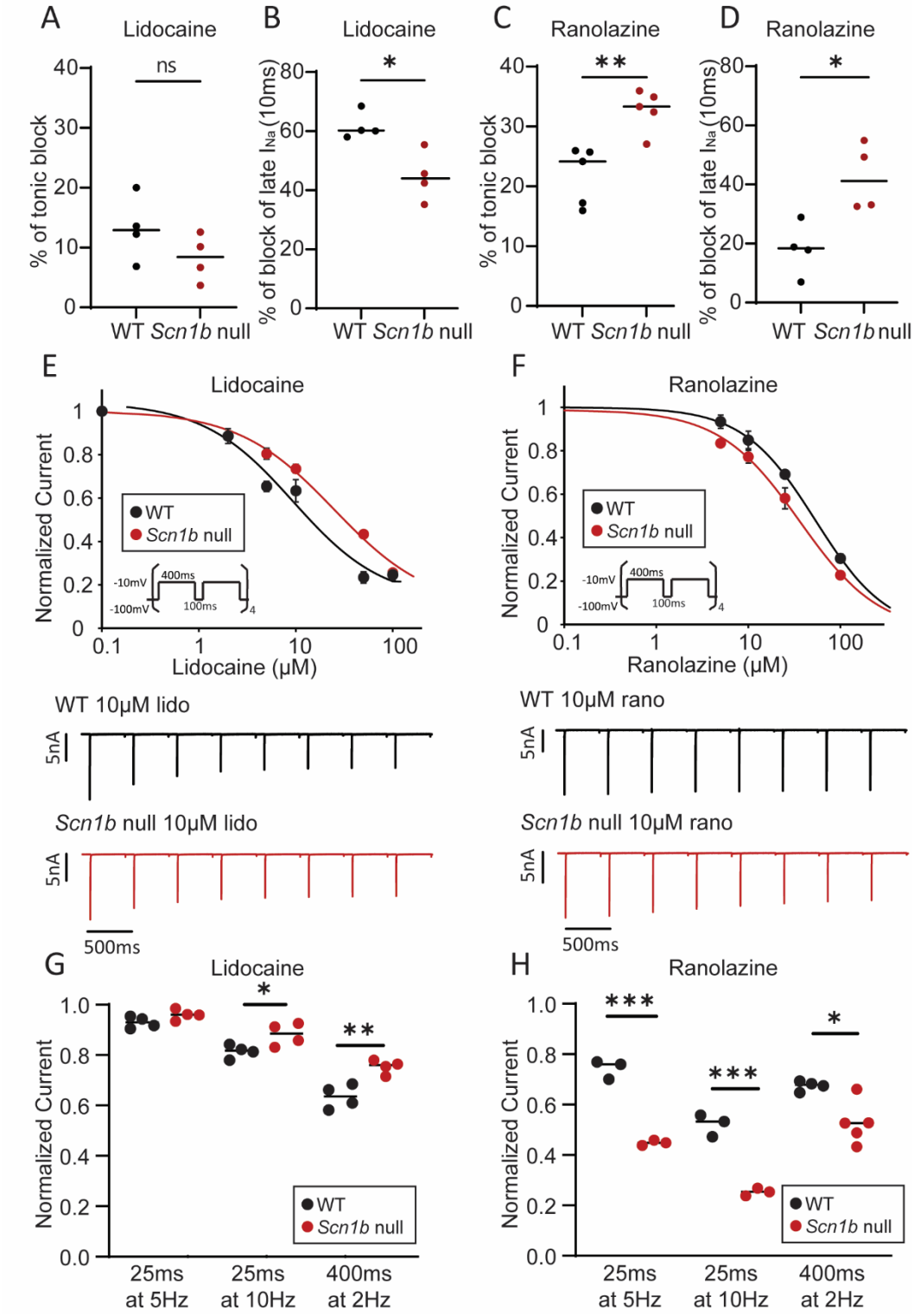

A. TB of I_{Na} by 100μM lidocaine is slightly reduced in *Scn1b* null, compared with WT, mouse LV myocytes.

B. Percentage of late I_{Na} block by 100μM lidocaine is markedly lower in *Scn1b* null, compared with WT, mouse LV myocytes. Late I_{Na} was measured 30ms after the onset of the depolarizing voltage step.

C. TB of I_{Na} by 100μM ranolazine is greater in *Scn1b* null, compared to WT, mouse LV myocytes.

D. Percentage of late I_{Na} block by 100μM ranolazine is greater in *Scn1b* null, compared to WT, mouse LV myocytes.

E. Dose-response curve (top) and example traces (bottom) for UDB of I_{Na} by lidocaine. UDB was examined by measuring I_{Na} evoked in response to 8 repetitive (400ms duration) depolarizations presented at 2Hz, which determines the initial rate of UDB. The EC_{50} for UDB of I_{Na} by lidocaine was lower in WT, compared with *Scn1b* null, suggesting that Navβ1 enhances the sensitivity to lidocaine.

F. Dose-response curve (top) and example traces (bottom) for UDB of I_{Na} by ranolazine. In contrast to lidocaine, the EC_{50} for UDB by ranolazine is higher in WT, compared to the *Scn1b* null, suggesting that Navβ1 reduces the effects of ranolazine.

G. Frequency-dependent UDB block of I_{Na} by 10μM lidocaine in WT and *Scn1b* null LV myocytes. UDB was assessed by measuring I_{Na} evoked by repetitive depolarizing pulses at 5Hz (25ms, 40 pulses), 10Hz (25ms, 40 pulses), and 2Hz (400ms, 8 pulses). Normalized currents indicate $I_{Na(last\text{-}pulse)}/I_{Na(first\text{-}pulse)}$.

H. Frequency-dependent UDB block of I_{Na} by 10μM ranolazine in WT and *Scn1b* null LV myocytes.

Each data set represents mean±SEM values of data acquired from 3-5 cells. Unpaired two-tailed Student's t-test was used to test significance. *, **, and *** represents p-value< 0.05, p-value<0.01, and p-value<0.001 accordingly.

Figure 6: ECG recordings from WT and *Scn1b* null mice before and after ranolazine or lidocaine injections.

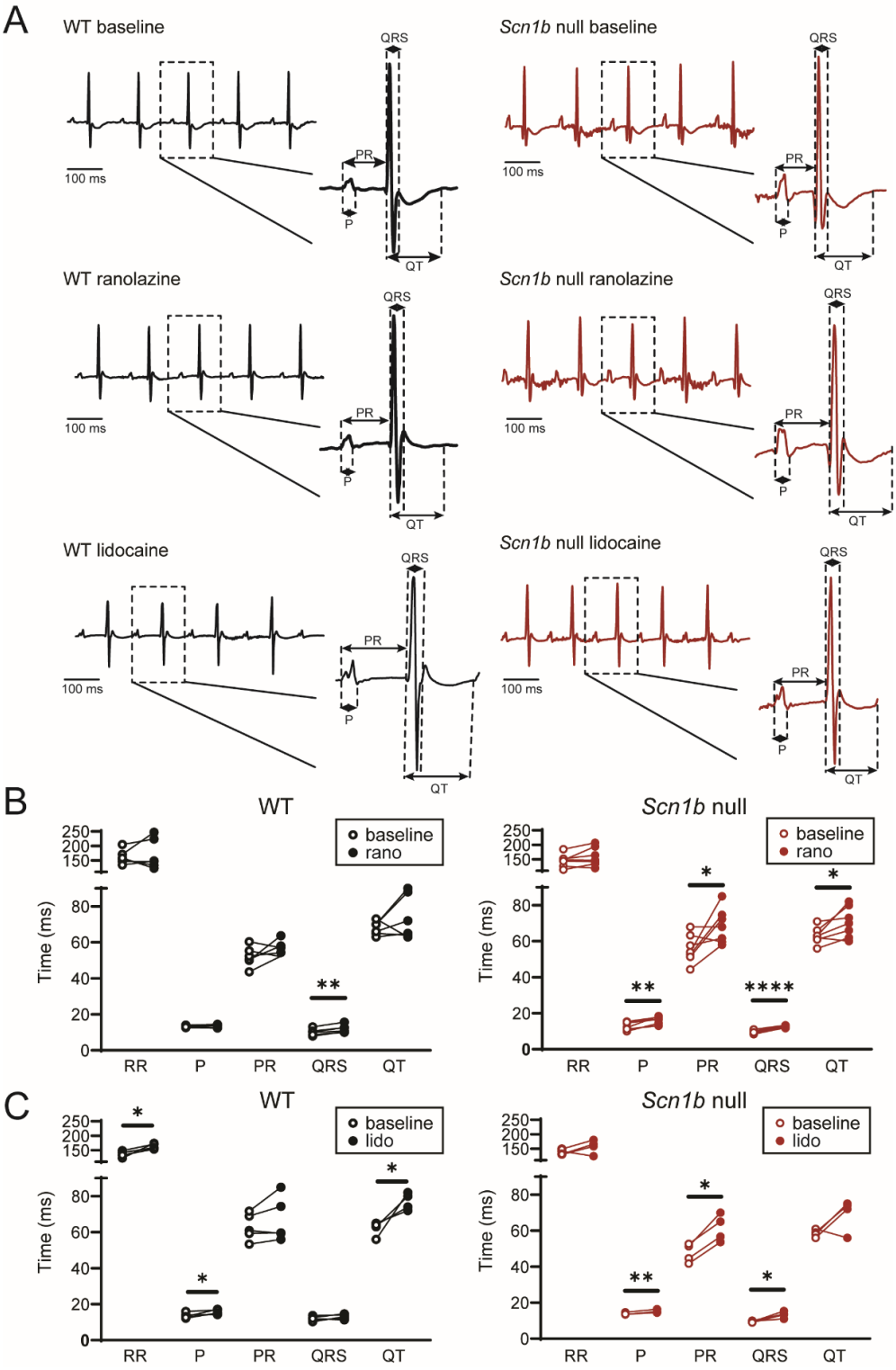

A. Representative ECG recordings obtained from WT and *Scn1b* null mice at baseline, post-ranolazine, and post-lidocaine are presented. The post-ranolazine and post-lidocaine data were recorded 10 minutes after the IP injections of ranolazine or lidocaine. P wave durations, PR, QRS, and QT intervals were measured as indicated in the insets.

B. Comparison of ECG parameters measured in WT (left panel) and *Scn1b* null (right panel) mice at baseline and 10 minutes after IP injections of ranolazine injection Ranolazine markedly prolonged the P wave duration and the PR interval in *Scn1b* null, but not in WT mice.

C. Comparison of ECG parameters measured in WT (left panel) and Scn1b null (right panel) mice at baseline and 10 minutes after IP injections of lidocaine. Lidocaine markedly prolonged the RR interval, P wave duration, and QT interval in WT mice. In *Scn1b* null mice, lidocaine also prolonged the P wave duration, and in addition, resulted in marked prolongation of the PR and QRS intervals.

Each data set represents data from 4-7 mice. The ECG parameters and statistical comparisons are shown in Supplement Table 1.

Figure 7: Regional differences in *SCN1B* expression in human atria and ventricles.

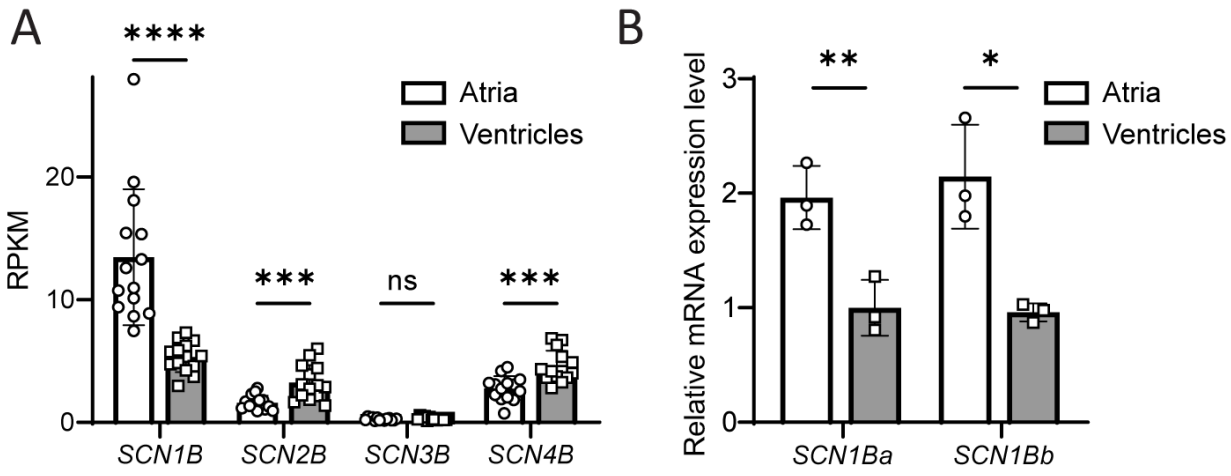

A. Extracted RNAseq data, expressed as RPKM (Reads Per Kilobase of exon per Million mapped reads), from analyses of sequencing data obtained from matched (n = 8) human ventricular and atrial tissue samples[44]. The *SCN1B* transcript is the most abundant of the Na$_V$β subunits expressed in both human atria and ventricles. In addition, *SCN1B* expression is ~3 fold higher in human atria, compared to ventricles, whereas both *SCN2B* and *SCN4B* are ~2 fold higher in human ventricles than atria.

B. The differential expression of *SCN1B* in human atria and ventricles was confirmed by quantitative PCR (qPCR) analyses of the same paired human atrial and ventricular tissue samples analyzed by RNAseq. In addition, qPCR analyses using primers that distinguish the s the two *SCN1B* variants, *SCN1Ba* and *SCN1Bb*, revealed that the relative expression levels of both (*SCN1Ba* and *SCN1Bb*) transcripts are higher in the atria than the ventricles.

Paired two-tailed Student's t-test was used to test significance. * represents p-value < 0.05, ** represents p-value <0.01, and *** represents p-value <0.001.